*Supporting information for*

# Isomeric organic-inorganic indium bromide single crystals with delayed and dual colour emission

Haichao Zhou,[a] Kiyonori Takahashi,[a,b] Takuya Okamoto,[a,b] Jianguo Pan,[c] Vasudevanpillai Biju[a,b]

## Experimental section

### Materials and methods

#### a) Materials

All chemicals were commercially obtained and used as received without further purification. 4-Piperidinopiperidine ($C_{10}H_{20}N_2$, >97%) and sodium bromide (NaBr, >99.5%) were obtained from Tokyo Chemical Industry (TCI). Indium (III) bromide ($InBr_3$, 99%) and aqueous hydrobromic acid (HBr, 47 wt%, >99.99%) were obtained from Sigma-Aldrich. 2-Propanol (IPA, >99.5%) was obtained from TCI.

#### b) Synthesis of isomeric crystals

We synthesized the crystals following a literature method.[41] First, a precursor solution was prepared by dissolving $InBr_3$ (1.2 mmol) in 7.8 mL of aqueous HBr (47 wt%) by stirring at room temperature (240 rpm). Subsequently, $C_{10}H_{20}N_2$ (1.2 mmol) was added to the $InBr_3$-HBr solution, and the mixture was stirred until complete dissolution. The resulting solution was heated to 120 °C and maintained at this temperature for 3 h. Crystal growth was induced by controlled cooling at 15 °C/h to room temperature. After standing undisturbed at room temperature for 2 h, the supernatant was decanted, and the obtained green-emitting crystals were dried under vacuum at room temperature. Yellow-emitting crystals were obtained under identical conditions, with the cooling rate reduced to 10 °C/h while all other parameters remained constant.

#### c) Preparation of saturated NaBr solution

A saturated NaBr solution was prepared by dissolving excess NaBr in 10 mL of IPA at room temperature. After standing for 3 h, the clear supernatant was collected and used for further experiments.

#### d) Optical measurements

Optical microscopic images, PL images, and PL spectra of samples mounted on an inverted optical microscope (Olympus, IX71) were measured using a digital camera (Olympus, STYLUS XZ-2) and a spectrometer (Ocean Optics, FLAME-S). The samples were excited with a 405 nm CW diode laser

(Thorlabs, 5–55 mW). The PL from the samples was collected using a 10× Olympus objective lens (NA = 0.60) and passed through a 420 or 480 nm long-pass filter. The sample temperature (from 298K to 323 K) was controlled and measured using a micro heat plate (KITAZATO, KM-1) and an infrared thermometer (KAIWEETS, Appolo 6), respectively. PL decays were acquired using a picosecond time-correlated single-phonon-counting (ps-TCSPC) system composed of 405 nm ps laser (PicoQuant, 500 kHz), an avalanche photodiode (APD, AQRI5, PerkinElmer), and a single-phonon-counting module (SPC-830, Becker and HicklGmBH). UV-vis absorption spectra were obtained in diffuse-reflectance mode using a Shimadzu UV-3600i spectrophotometer with an integrating sphere. PLQY and PL excitation spectra (PLE) were measured using the FLS-980 fluorescence spectrometer. Temperature-dependent photoluminescence spectra from 80 to 300 K were collected using the FLS 980.Temperature-dependent PL measurements of single crystals, including steady-state PL spectra and PLQY, were carried out using a Horiba FLS1000 fluorescence spectrometer equipped with a 450 W ozone-free xenon lamp.

**e) Scanning electron microscope (SEM)–energy dispersive X-ray (EDX) measurements**

The topographical images were obtained using an SEM (SU8230, Hitachi) operated at an acceleration voltage of 1 kV. EDX elemental mapping was performed using a Bruker SEM-EDX (QUANTAX EDS) operated at 10 kV. The as-prepared crystals were directly mounted on a borosilicate glass substrate for SEM and EDX measurements, without additional conductive coating. The Br/In ratios were estimated from the EDX peak intensities of Br (Kα, 11.9 keV) and Cu (Lα, 3.3 keV).

**f) Structural characterization**

Single Crystal X-ray Diffraction (SCXRD) data were collected on a Rigaku XtaLAB Synergy diffractometer equipped with a HyPix-6000 area detector at 100K, using multilayer mirror–monochromated Mo Kα radiation (λ = 0.71073 Å). A suitable single crystal was mounted on a MicroMounts™ tip (MiTeGen) using Paratone 8277 oil (Hampton Research). Multiscan absorption corrections were applied to the reflection data. Crystal structure solution was carried out using Olex2, and full-matrix least-squares refinement on $F^2$ was performed using Olex2. Structural visualization and simulated powder X-ray diffraction (PXRD) patterns were generated using the VESTA software, based on the refined crystal structures, employing Cu Kα radiation (λ = 1.5406 Å). Experimental PXRD patterns were recorded on a Rigaku SmartLab diffractometer with Cu Kα radiation (λ = 1.5406 Å). The single crystals were gently ground into powders prior to measurement.

**g) Thermal analysis**

The STA 2500 Regulus NETZSCH simultaneous thermal analyzer was used for DTA analysis of the crystals, and the temperature was increased from 20 °C to 600 °C at 10 °C $min^{-1}$ under a nitrogen atmosphere.

**h) Density functional theory DFT) calculations (**

We have employed the first-principles tool, the Vienna Ab initio Simulation Package (VASP),[1,2] and performed all DFT calculations within the generalized gradient approximation (GGA) using the Perdew-Burke-Ernzerhof (PBE)[3] formulation. We have chosen the projected augmented wave (PAW) potentials[4,5] to describe the ionic cores and have included valence electrons in a plane-wave basis set with a kinetic-energy cutoff of 450 eV. Partial occupancies of the Kohn−Sham orbitals were allowed using the Gaussian smearing method and a width of 0.05 eV. For the optimization of both geometry and lattice size, the Brillouin zone integration was performed with a 0.04 $Å^{-1}$ *k*-mesh Gamma-centered sampling.[6] The self-consistent calculations applied a convergence energy threshold of $10^{-5}$ eV. The equilibrium geometries and lattice constants were optimized with maximum stress on each atom within 0.02 eV $Å^{-1}$. The weak interaction was described using the DFT+D3 method with the empirical correction in Grimme's scheme [7, 8]

**Table S1** Comparison of In-Br bonds in the green- and yellow-emitting crystals.

| | Green-emitting crystals | | Yellow-emitting crystals | |
|---|---|---|---|---|
| | Bond length (Å) | Bond angle (°) | Bond length (Å) | Bond angle (°) |
| Tetrahedra | 2.4726; 2.4735; 2.4784; 2.4897 | 106.49; 107.49; 109.61; 110.72; 111.02; 111.35 | 2.4726; 2.4732; 2.4819; 2.4887 | 106.50; 107.47; 109.53; 110.82; 110.99; 111.37 |
| Corner-sharing octahedra | 2.6584; 2.6850; 2.7003 | 88.65; 89.35; 89.63; 90.37; 90.65; 91.35 | 2.6543; 2.6625; 2.6997 | 88.21; 89.36; 89.65; 90.46; 90.64; 91.79 |
| Face-sharing octahedra | 2.6542; 2.6612; 2.7023 | 88.19; 89.37; 89.51; 90.49; 90.66; 91.81 | 2.6587; 2.6859; 2.6994 | 88.69; 89.40; 89.61; 90.39; 90.60; 91.30 |

**Table S2** PL decay components of a broken green-emission crystal.

| | Before breaking (ns) | After breaking 0 min (ns) | After breaking 4 min (ns) |
|---|---|---|---|
| $a_1$ | 1323.88 | 4425.81 | 2925.25 |
| $\tau_1$ | 2.08 (85.5%) | 2.20 (90.7%) | 2.10 (89.9%) |
| $a_2$ | 223.91 | 453.18 | 327.85 |
| $\tau_2$ | 5.93 (14.5%) | 7.39 (9.3%) | 7.71 (10.1%) |
| $\tau_{av}$ | 2.64 | 2.68 | 2.66 |

**Table S3** PL decay components of a broken yellow-emission crystal.

| | Before breaking (ns) | After breaking 0 min (ns) | After breaking 4 min (ns) |
|---|---|---|---|
| $a_1$ | 1505.12 | 2027.77 | 1235.63 |
| $\tau_1$ | 2.14 (88.2%) | 2.45 (97.6%) | 2.47 (96.9%) |
| $a_2$ | 201.99 | 48.90 | 40.03 |
| $\tau_2$ | 6.58 (11.8%) | 48.78 (2.4%) | 57.12 (3.1%) |
| $\tau_{av}$ | 2.66 | 3.54 | 4.19 |

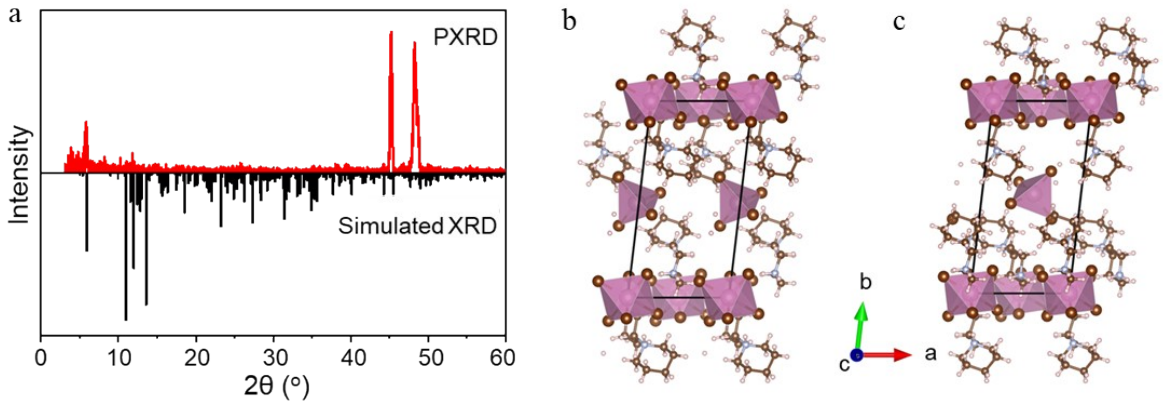


**Fig. S1** (a) PXRD and Simulated XRD patterns of the green-emitting isomer. (b, c) The SCXRD structures of the primitive unit cells of (b) green- and (c) yellow-emitting crystals.

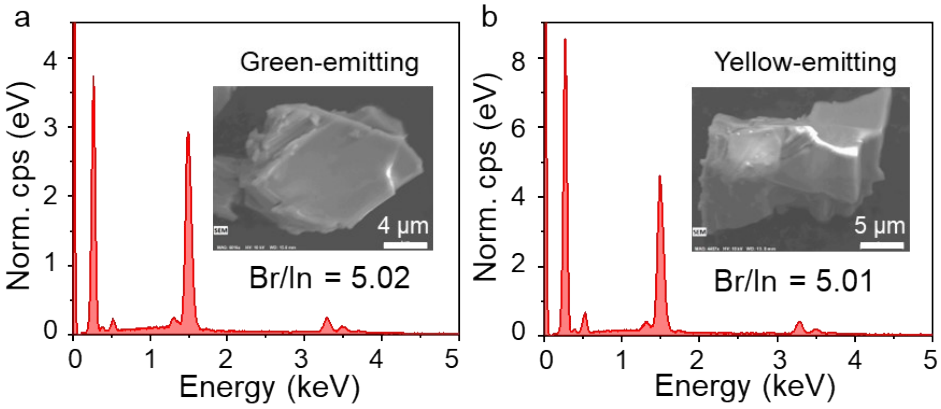


**Fig. S2** SEM images and EDX spectra of (a) green- and (b) yellow-emitting crystals.

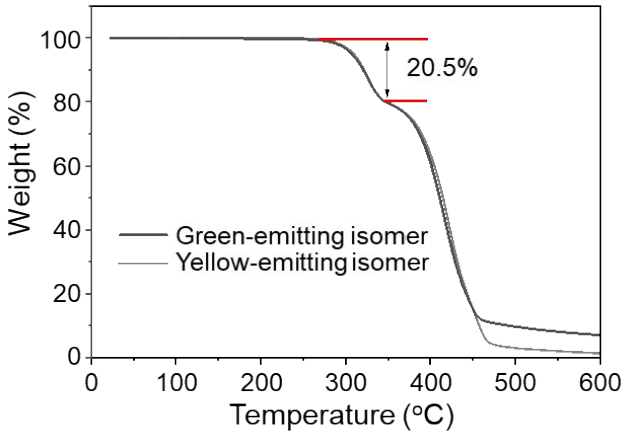


**Fig. S3** DTA of green- and yellow-emitting crystals.

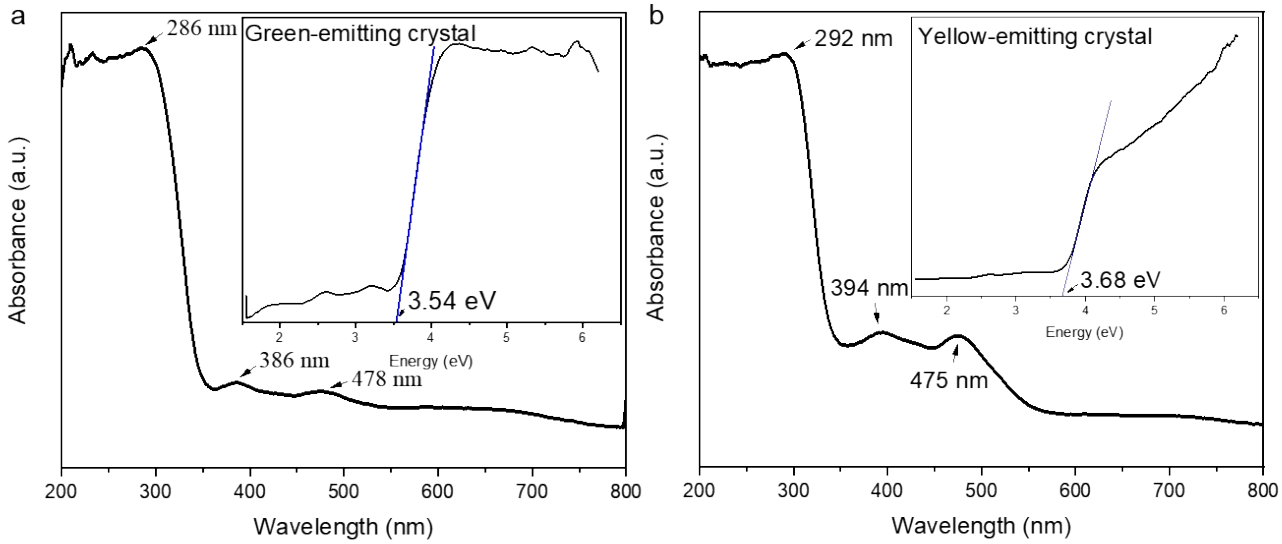


**Fig. S4** Absorption spectra of (a) green- and (b) yellow-emitting crystals. Insets are optical band gaps of the isomers.

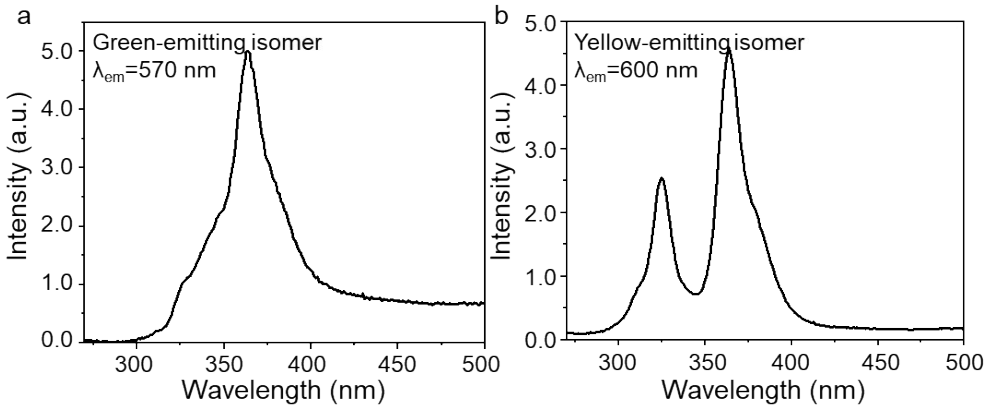


**Fig. S5** PL excitation spectra of (a) green- and (b) yellow-emitting crystals.

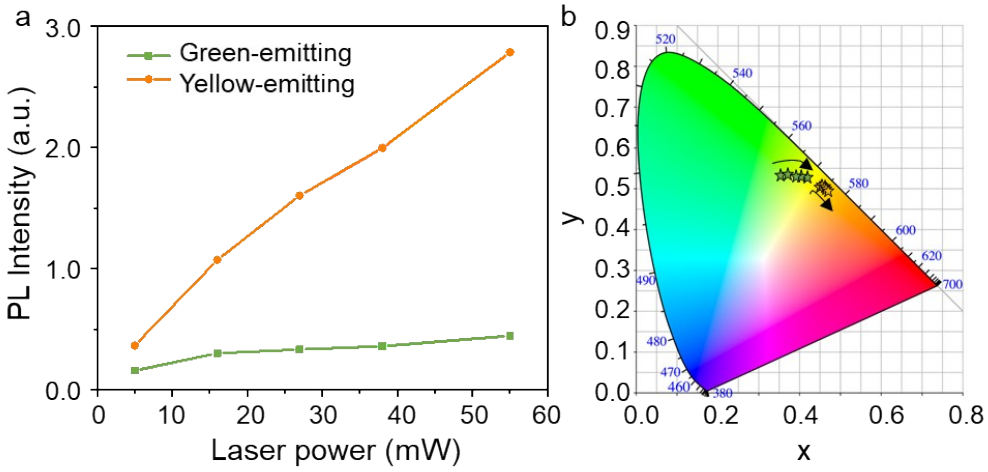


**Fig. S6** (a) Excitation power–dependent PL intensities of green- and yellow-emitting crystals measured under identical experimental conditions. (b) CIE chromaticity coordinates of the green- and yellow-emitting crystals derived from their PL emission spectra.

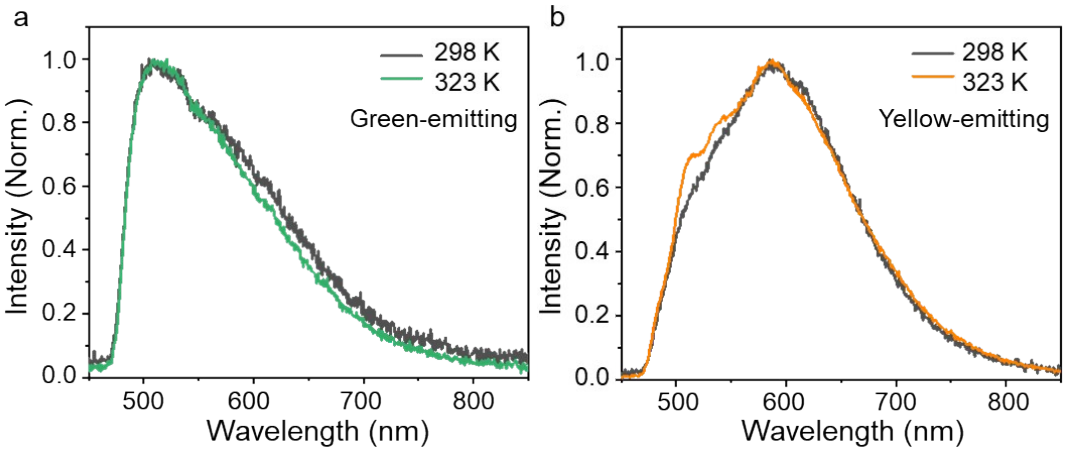


**Fig. S7** PL spectra of (a) green- and (b) yellow-emitting crystals at 298 K and 323 K.

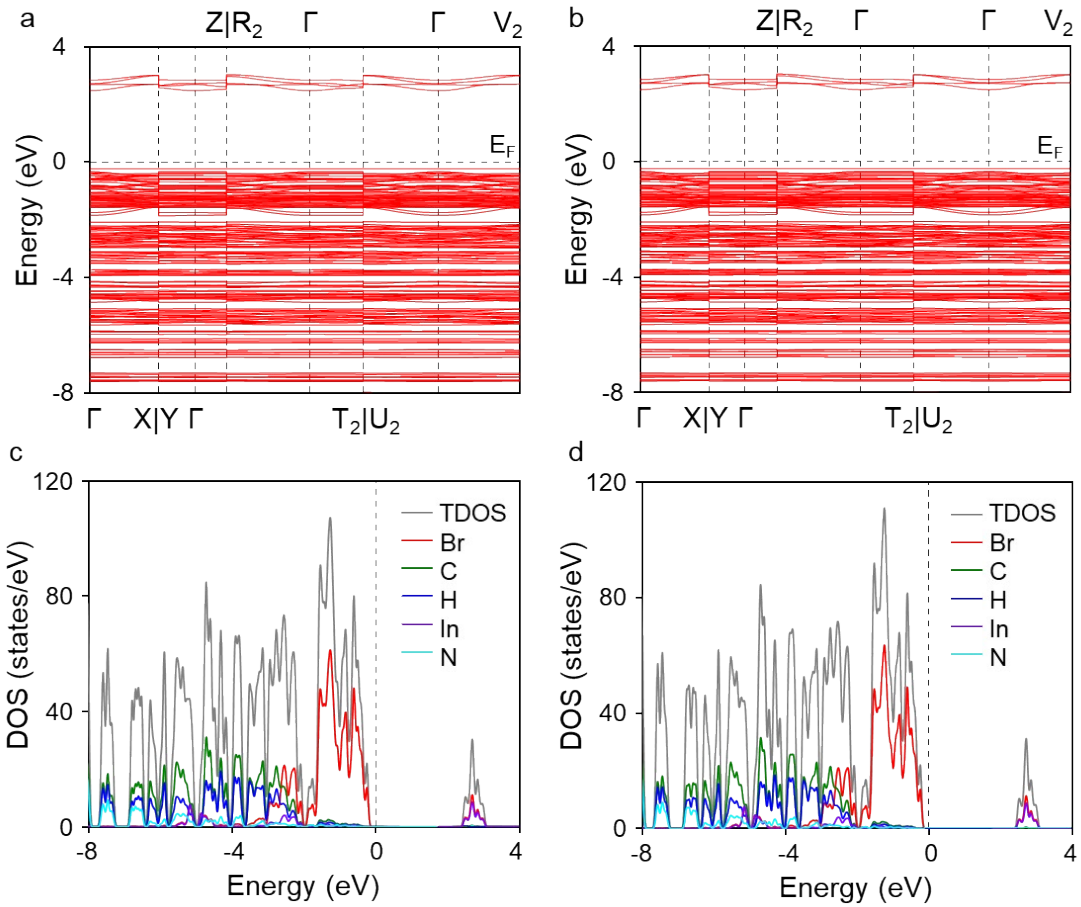


**Fig. S8** Band structure of (a) green- and (b) yellow-emitting isomers. Total and partial density of states (DOS) of (c) green- and (d) yellow-emitting isomers.

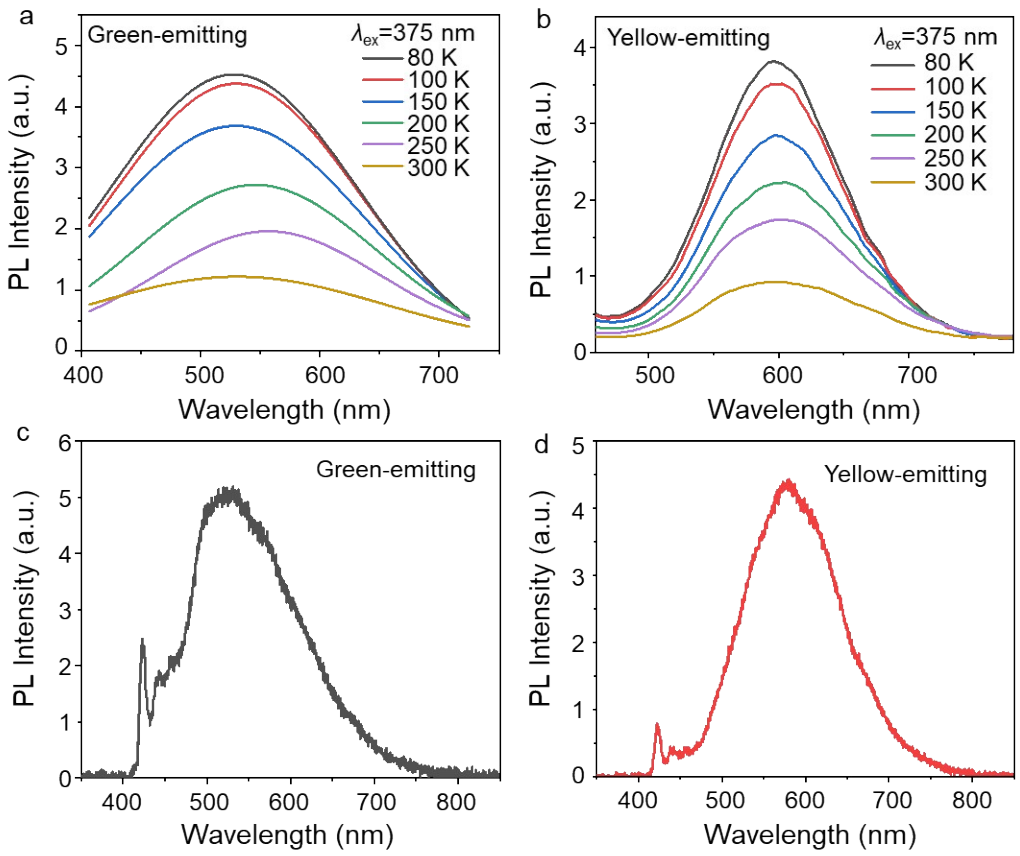


**Fig. S9** (a, b) Temperature-dependent PL spectra of (a) green- and (b) yellow-emitting crystals recorded under 365 nm excitation. The background due to 375 nm excitation was removed by deconvolution. (c, d) PL spectra of (c) green- and (d) yellow-emitting crystals under 365 nm. The weak background signal in the 410-460 nm range is due to the excitation source.

## References


1. G. Kresse and J. Furthmuller. *Comput. Mater.*, 1996, **6**, 15−50.
2. G. Kresse and J. Furthmüller. *Phys. Rev. B* 1996, **54**, 11169−11186.
3. J. P. Perdew; K. Burke and M. Ernzerhof. *Phys. Rev. Lett.*, 1996, **77**, 3865−3868.
4. G. Kresse and D. Joubert. *Phys. Rev. B*, 1999, **59**, 1758-1775.
5. P. E. Blöchl. *Phys. Rev. B*, 1994, **50**, 17953-17979.
6. H. J. Monkhorst and J. D. Pack. *Phys. Rev. B*, 1976, *13(12)*, 5188.
7. S. Grimme, J. Antony, S. Ehrlich and S. Krieg, *J. Chem. Phys.*, 2010, **132**, 154104.
8. S. Grimme, S. Ehrlich and L. Goerigk, *J. Comp. Chem.*, 2011, **32**, 1456.